RSC Advances

PAPER

View Article Online
View Journal | View Issue

Cite this: *RSC Adv.*, 2017, 7, 52165

Laser irradiation-induced construction of Pt/Ag bimetallic nanourchins with improved electrocatalytic properties†

Hua Zhang, Ming Chen, * Linlin Xu, Wanda Hou, Xiangdong Liu* and Feng Chen *

Received 21st August 2017
Accepted 30th October 2017

DOI: 10.1039/c7ra09242c

rsc.li/rsc-advances

Platinum (Pt)-based nanomaterials with rough surfaces are regarded as promising catalysts in fuel cells. Herein, we report a versatile and green strategy to synthesize Pt/Ag (Pt : Ag ∼ 9 : 1) bimetallic nanourchins with mean size of ∼70 nm by laser irradiation of Ag_2S/Ag nanoparticles in a potassium chloroplatinate (K_2PtCl_4) water solution. The distinctive advantages of this novel anisotropic synthesis are as follows: (I) the enhanced anisotropic replacement reaction derived by laser-induced photothermal effect on the nanoseeds gives rise to the anisotropic deposition of Pt atoms and then the formation of rugged intermediate precursors, and (II) the subsequent anisotropic overgrowth of Pt and Ag atoms *via* enhanced co-reduction reaction motivated by laser-induced surface plasmon resonance will preferentially occur at protrusion surfaces on the intermediate precursors. Without any binder/stabilizer/capping additives, the pure Pt/Ag bimetallic nanourchins exhibit excellent long-term stability during repeated cyclic voltammogram (CV) tests. Electrochemically active surface area (ECSA) tests illustrate that the novel catalysts exhibit a negligible loss of 0.2% after 1500 repeated applications, while that of commercial Pt/C catalyst is 78.7% after 1000 cycles. Moreover, the ECSA-normalized CV curve and chronoamperometric (CA) measurements reveal that Pt/Ag bimetallic nanourchins possess enhanced electrocatalytic activity and stability in the methanol oxidation reaction. Correspondingly, the mass-normalized (mass of Pt) CVs show that the peak of mass current is about 302.35 mA mg_{Pt}^{-1}, which is 5.2 times higher than that of commercial Pt/C catalyst. For the entire time course (2000 s), the CA curves show that the current density is about 0.38 mA cm_{Pt}^{-2}, while that of commercial Pt/C electrocatalyst is 0.014 mA cm_{Pt}^{-2}. Thus the Pt/Ag bimetallic nanourchins should be established as an advanced electrocatalyst for direct methanol fuel cell application. These findings will also stimulate the investigation of using laser light as an effective tool for sculpting pure functional metal-based nanomaterials.

Introduction

Among all the noble metals, platinum (Pt) with intrinsic electronic structure and intriguing catalytic properties has been widely used as an excellent heterogeneous catalyst, and attracted a tremendous amount interest for oxygen reduction reaction in direct methanol fuel cell (DMFC) applications.[1–6] Increasing evidence has shown that Pt-based bimetallic nanomaterials with complex compositions exhibit improved electrocatalytic activities, and much higher than that of monometallic Pt nanomaterials, owing to the pronounced intermetallic synergies.[2,3] Moreover, the corresponding structures also play an important role in their electrocatalytic properties. Compared with solid interiors and smooth surfaces, various rugged Pt-based bimetallic nanostructures such as sponge-like Au/Pt nanomaterial,[2] hollow PtPd nanoparticles,[7] AuPt nanodendrites,[8] porous Au@Pt and Pt@Fe nanocrystals,[1,9] flowerlike Pt-based nanorods,[10] and porous Pt–Pd nanowires[11] have been established as excellent electrocatalysts, owing to their lower density, larger specific surface area and higher permeability.

It is noted that most previous works mainly focused on the synthesis of Pt-based nanomaterials based on a precursor reaction or ligand exchange *via* complicated polymer stabilizers and organic structure-directing additives, including octadecyltrimethylammonium chloride,[1] Pluronic F127,[3,7] poly(ViEtImBr),[8] phenylalanine,[9] and poly(*N*-vinyl-2-pyrrolidone).[11] These additives lead to the presence of organic contamination on the surface of Pt-based nanomaterials. There are always required extra purification procedures to eliminate excess residual materials before being processed toward functional products. Unfortunately, the removal and cleaning of the residual materials is very difficult and costly. Usually, the

---

School of Physics, State Key Laboratory of Crystal Materials, Shandong University, Jinan 250100, China. E-mail: chenming@sdu.edu.cn; xdliu@sdu.edu.cn; drfchen@sdu.edu.cn

† Electronic supplementary information (ESI) available. See DOI: 10.1039/c7ra09242c

products should be cleaned by centrifugation, and thoroughly washed many times by ultrapure water or ethanol.[1,3,7,8,11] In order to improve the nanomaterials' purity and reduce the use of those complicated additives, a facile, green and efficient method that can create pure nanostructures is urgently desired, which is also highly favorable for various potential applications.

Laser ablation/irradiation-induced synthesis of diverse nanomaterials in liquid is an emerging technique.[12–14] Superior to traditional synthesis, the fascinating feature is that the laser-induced photothermal treatment and enhanced photochemical reaction without any binder/stabilizer/capping additives, *etc.*, can be used as an effective tool for manipulation of nanomaterial shape, size and composition with a relatively high level of control.[13] For example, well-defined ZnO, TiO_2 and CuO submicrometer-scale spheres have been successfully realized by KrF (248 nm) laser irradiation of irregular ZnO, TiO_2 and CuO powder in distilled water.[15] Most recently, single crystal Au nanoparticles with ultra-smooth and perfect spherical shape have also been obtained by non-focused laser irradiation *via* a photothermal melting–evaporation model.[16] Moreover, our group has confirmed that laser beam irradiation in liquid has become a powerful and green tool for constructing metal-based nanoarchitectures such as mono-dispersed Ag_2S/Ag nanoparticles,[12] ZnS/Zn nanocages,[13] and CuS and Ag/Au nanodendrites.[14,15] Herein, we demonstrate experimentally that Pt/Ag (Pt : Ag ∼ 9 : 1) bimetallic nanourchins can be successfully constructed by laser irradiation of Ag_2S/Ag nanoseeds in K_2PtCl_4 water solution. To reveal the anisotropic growth mechanism, an enhanced replacement reaction derived by laser-induced photothermal effect and then enhanced co-reduction of Pt and Ag ions *via* excited electrons generated by laser-induced optical excitation of surface plasmon resonance (SPR) have been proposed. Without any binder/stabilizer/capping additives, the obtained Pt/Ag bimetallic nanourchins provide pronounced electrocatalytic stability during cyclic voltammogram (CV) measurements. Correspondingly, electrochemically active surface area (ECSA) results show that the novel catalysts exhibit a negligible loss of 0.2% after 1500 repeated tests, while that of commercial Pt/C catalyst is 78.7% after 1000 cycles. Based on the ECSA-normalized CV curve and chronoamperometric (CA) measurements, as expected, the Pt/Ag bimetallic nanourchins provide improved electrocatalytic activity and stability for the methanol oxidation reaction (MOR). The mass-normalized (mass of Pt) CV results show that the peak of mass current is about 302.35 mA mg_{pt}^{-1}, which is 5.2 times higher than that of commercial Pt/C catalyst. The CA curves indicate that the current density is ∼0.38 mA cm_{Pt}^{-2}, while that of commercial Pt/C electrocatalyst is 0.014 mA cm_{Pt}^{-2}. There is no doubt that the pure Pt/Ag nanourchins will be very suitable for DMFC application.

Experimental details

Ag_2S/Ag nanoparticles were fabricated firstly, in order to provide nanoseeds for further fabrication of Pt/Ag bimetallic nanourchins. The preparation of the mono-dispersed Ag_2S/Ag nanoparticles was conducted by the laser ablation of pure Ag target in thioacetamide (TAA) solution, which was reported in our previous work.[17] The experimental setup is similar to that described in our previous studies.[18–20] Briefly, a well-polished Ag metal target (10 mm in diameter and 2 mm in thickness) was placed on the bottom of a glass dish rotating with speed of ∼300 rpm that was filled with 2.5 mm depth of liquid solution containing 0.2 M TAA and 8 mL distilled water. The TAA can provide the sulfur source for the construction of Ag_2S materials. A 1064 nm laser beam with a pulse duration of 10 ns and 10 Hz repetition rate was originated from a Q-switched Nd-YAG (yttrium aluminum garnet) equipment (Quanta Ray, Spectra Physics). The laser beam with power density of 6 GW cm^{-2} was focused on the Ag target with average spot size of ∼500 μm by a quartz lens with 65 mm focal length. Then, Ag_2S/Ag nanoseeds were centrifuged at 10 000 rpm for 10 minutes in an ultracentrifuge. Then 1 mg Ag_2S/Ag nanomaterials were added to another 10 mL solution including 200 μL of 0.05 M K_2PtCl_4. Finally, Pt/Ag bimetallic nanourchins were further constructed *via* laser irradiation of the Ag_2S/Ag nanoseeds in the mixed solution. A continuous low-power (250 mW) 532 nm laser beam with average spot size of 1.5 cm was selected for fabricating the Pt/Ag bimetallic nanourchins. After laser irradiation for 3 hours, the products were carefully washed in distilled water, and centrifuged at 5000 rpm for 10 minutes in an ultracentrifuge. The sediments were dropped on a copper mesh and dried in an oven at room temperature for observation by transmission electron microscopy (TEM; JEOL-JEM-2100F). In addition, the morphology and chemical composition were investigated by a field emission scanning electron microscope (SEM; Hitachi, S-4800) equipped with an energy dispersive X-ray spectroscopy (EDS) facility. The crystallographic investigations of the products were conducted with X-ray diffraction (XRD) patterns (Rigaku, RINT-2500VHF) using Cu Kα radiation ($\lambda = 0.15406$ nm). The detailed sample compositions were studied by X-ray photoelectron spectroscopy (XPS) using a PHI Quantera SXM with an Al Kα = 280.00 eV excitation source. In a typical electrochemical test, 10 mL of Ag/Pt bimetallic nanourchin solution was centrifuged at 5000 rpm for 10 min, and finally redispersed in 0.5 mL of water to form a suspension. 5 μL Nafion (5%) was added into the suspension and then mixed uniformly by ultrasound waves to form a slurry. 5 μL of the slurry was dropped onto a glass carbon electrode and dried naturally at ambient temperature. The Pt masses of Ag/Pt nanourchins and commercial Pt/C on the glass carbon electrode were 10 μg and 8 μg, respectively. CVs were recorded by using an LK2005 electrochemical workstation equipped with a three-electrode system. The working electrode was a glassy carbon electrode (3 mm in diameter), a Pt sheet was the counter electrode, and a saturated calomel electrode (SCE) was the reference electrode. Typical CVs for different catalysts were obtained in 0.5 M H_2SO_4 solution at a sweep rate of 50 mV s^{-1}.

Results and discussion

Fig. 1 shows a typical schematic of our experimental configuration. In a typical experiment, mono-dispersed Ag_2S/Ag nanoparticles were firstly fabricated by a laser ablation approach, which was reported in our recent work.[17] The Pt/Ag bimetallic

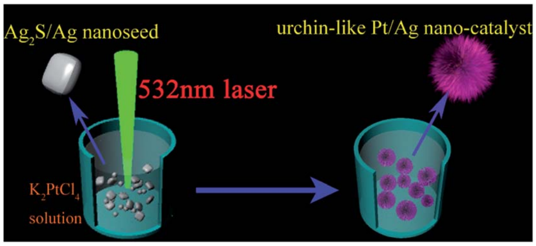

Fig. 1 A schematic diagram of the overall procedure for synthesizing the Pt/Ag bimetallic nanourchins.

nanourchins were further constructed by continuous 532 nm laser irradiation. The morphologies of the Ag_2S/Ag nanoparticles are demonstrated by SEM and TEM, as shown in Fig. 2a and b. The results illustrate that numerous monodispersed quasi-cubical-like Ag_2S/Ag nanoparticles with average size of ~45 nm are likely to be fabricated individually and are not hinge jointed. The HRTEM image (Fig. 2c) reveals the lattice fringes with a *d*-spacing of 0.393 nm and 0.238 nm that could be indexed with reference to the Ag_2S (101) and Ag (111) plane structures, respectively. Then, the hybrid Ag_2S/Ag structures were irradiated by a laser beam to lead to the anisotropic growth of Pt species on the precursors.

After 532 nm laser irradiation of the preliminary Ag_2S/Ag nanoparticles in K_2PtCl_4 solution, the final products were obtained, as illustrated in Fig. 3. The typical SEM image (Fig. 3a) shows that the morphologies of the final nanomaterials are spherical-shaped architectures with average size of ~70 nm, which are larger than the original Ag_2S/Ag nanoparticles. Compared with the smooth precursors (Fig. 2a), a closer view of these nanostructures reveals that the surfaces are very rough and rugged structures. Moreover, the corresponding TEM image in Fig. 3b exhibits urchin-shaped structures with dense nano-protrusions formed on the core of the solid bodies. In addition, crystallographic investigations were conducted using XRD (Fig. 3c). A series of diffraction peaks originating from Ag_2S/Ag structures disappeared in the pattern of the products. Meanwhile, three relatively strong peaks at 40.01°, 46.77° and 67.75° should be indexed with reference to (111), (200) and (220) planes in Pt face-centered-cubic structures (JCPDS, no. 70-2057). The EDS result (Fig. 3d) also demonstrates that the obtained products are mainly composed of Pt and Ag (very few S species). The relative ratio of Pt, Ag and S is calculated as about 91.07 : 8.28 : 0.65. Compared with the 25.6% S composition in the original Ag_2S/Ag nanoseeds (Fig. S1†), the very small S content in the final product implies that major S species have been decomposed from the nanostructure. Moreover, the product composition will be also further verified in the following section.

Moreover, an enlarged TEM image of the structural detail of an individual nanourchin is illustrated in Fig. 4a. The morphology in Fig. 4a further confirms that the obtained product has a rugged structure with plentiful nano-protrusions formed on the surface. Correspondingly, the HRTEM image shows that the lattice fringes with a spacing of 0.227 nm can be assigned to the Pt (111) plane (inset in Fig. 4a). The cross-sectional compositional line profiles in Fig. 4b clearly show the Pt, Ag and S element distributions. The results reveal that the nanourchin is composed mainly of Pt (91.1%) and Ag (8.3%). The very small amount of S in the product is about 0.6%. Moreover, the elemental mapping images (Fig. 4c) also reveal that the product is indeed composed of Pt, Ag and S elements. The relative ratio is about 91.11 : 8.35 : 0.54, respectively, which is also consistent with the compositional line profiles (Fig. 4b) and EDS results (Fig. 3d). Moreover, the elemental mapping images coupled with the compositional line profiles clearly illustrate the uniform distributions of Pt and Ag elements throughout the nanourchins, which are nearly overlapped and homogeneously alloyed within an individual nanourchin. Different from the core–shell structure, the distributions of Pt and Ag compositions in an individual nanourchin have almost the same profile width, supporting the formation of bimetallic Pt/Ag nanostructure.

Additionally, the purity and surface composition of the obtained Pt/Ag bimetallic nanourchins were further examined by XPS. As shown in Fig. 5a, the strong peaks of Pt and Ag, as well as the weaker peaks of S were detected in the XPS spectrum. The binding energies were calibrated by reference to the C 1s peak at 284.8 eV to reduce the sample charge effect.[17] The doublet feature of Ag $3d_{5/2}$ (Ag ions at 367.3 eV) and Ag $3d_{3/2}$ (Ag atoms at 373.4 eV) with intensity ratio of 3 : 2 is attributed to the spin–orbit separation; these two peaks are both peaks of Ag^0 (Fig. 5b).[21] The Pt 4f spectra indicate that the Pt 4f region can be divided into two pairs of doublets (Fig. 5c). The doublet peaks of Pt $4f_{7/2}$ and Pt $4f_{5/2}$ at 70.9 and 74.1 eV can be assigned to metal Pt atoms. The weaker doublet is located at 71.8 eV and 75.0 eV, which can be attributed to Pt in oxidized forms.[8,22–24] On the

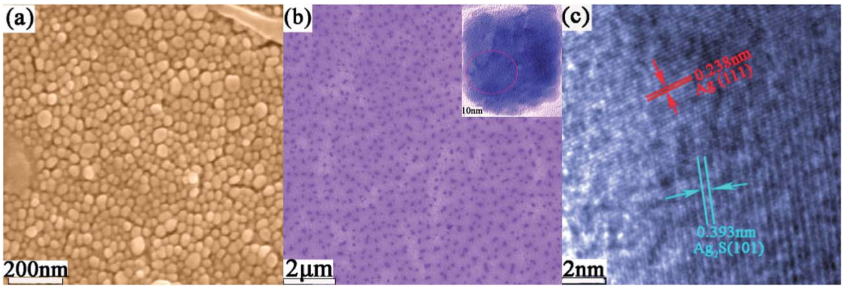

Fig. 2 (a) SEM and (b) TEM images of Ag_2S/Ag nanoparticles. (c) HRTEM image of Ag_2S/Ag nanostructure.

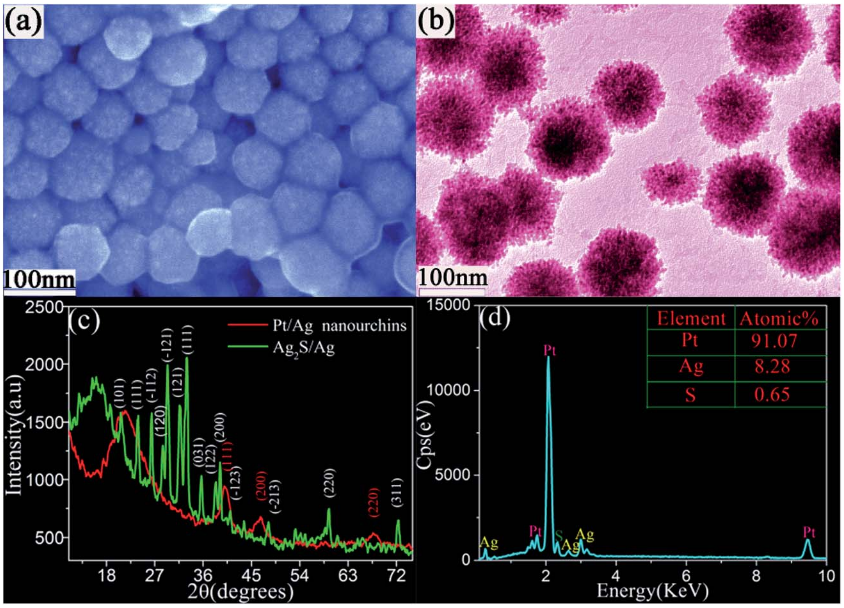

Fig. 3 Typical (a) SEM and (b) TEM images of the Pt/Ag bimetallic nanourchins obtained by 532 nm laser irradiation of Ag_2S/Ag nanoseeds for 3 hours. (c) XRD patterns of Ag_2S/Ag nanoparticles and the Pt/Ag bimetallic nanourchins. (d) The EDS analysis of Pt/Ag bimetallic nanourchins.

other hand, no additional impurities or organic contamination on the surface can be detected by XPS, supporting the formation of pure nanomaterials using the method presented in this paper. Moreover, based on the integrated area and sensitivity factors of Pt 4f and Ag 3d, the surface atomic ratio of Pt and Ag atoms is calculated to be about 9 : 1, which is also consistent with the individual nanourchin composition and EDS result. In summary, based on the above experimental results, it is reasonable to deduce that the obtained product should be pure bimetallic Pt/Ag (Pt : Ag ∼ 9 : 1) nanourchins.

In this section, we will qualitatively describe the possible growth of the mono-dispersed Pt/Ag bimetallic nanourchins. Firstly, the replacement reaction between Ag element in Ag_2S/Ag seeds and Pt^{2+} ions in solution will play a critical role in the initial stage. So, the deposition of Pt atoms on the nanoseeds and dissolution of Ag and S ions in solution will simultaneously occur in the early stage. The distinctive feature of our synthesis strategy is that laser-induced photothermal treatment can significantly accelerate the replacement reaction rate on irradiated surface in colloidal solution. In this way, compared with unirradiated regions, the enhanced replacement reaction should result in anisotropic deposition of Pt atoms and then the formation of intermediate products with rough and rugged surface structures. This is very different from a homogeneous chemical reaction. To verify it, the rugged nanoarchitectures obtained by laser irradiation for 40 minutes are shown in Fig. S2.† The cross-sectional compositional line profiles in Fig. S2† illustrate that the intermediate product is mainly composed of 97.84% Pt species, supporting the dissolution of Ag and S elements by replacement reaction in the initial stage. Therefore, the enhanced replacement reaction derived by laser-induced photothermal effect plays an important role in the formation of rugged intermediate products. Subsequently, the overgrowth of Pt and Ag atoms by co-reduction of Pt^{2+} ions and Ag^+ ions (originating from the replacement reaction) with weak reducing agent of ascorbic acid (AA) will occur during the laser irradiation process. In the same way, the laser-induced photothermal effect will also enhance the co-reduction process on the

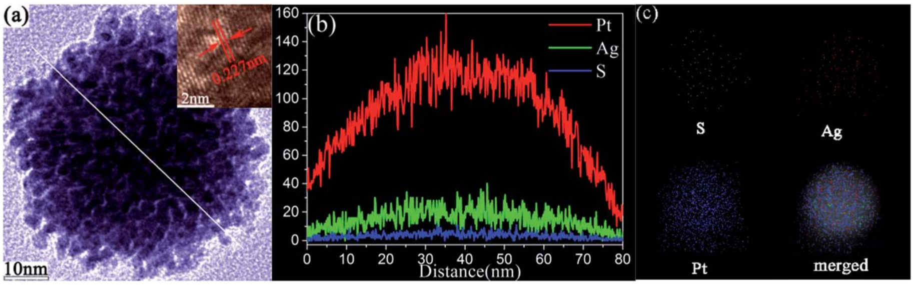

Fig. 4 (a) An enlarged TEM image of an individual Pt/Ag bimetallic nanourchin. Inset shows the HRTEM image. (b) The cross-sectional compositional line profiles of the Pt/Ag bimetallic nanourchin. (c) The corresponding elemental mapping images of the Pt/Ag bimetallic nanourchin.

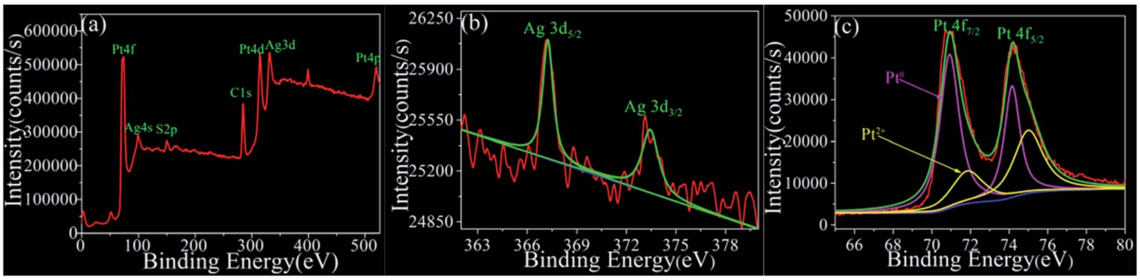

Fig. 5 (a) XPS survey spectrum of the Pt/Ag bimetallic nanourchins. Detailed spectra of (b) Ag and (c) Pt.

nanoseed surfaces. Meanwhile, the laser irradiation-induced effective SPR on the surface of Ag-based nanoseeds can also lead to an additional reduction of Pt ions on the nanoseeds. The absorption spectrum shows that the Ag-based nanostructures are anticipated to provide an ideal SPR in the visible region (~450 nm absorption, Fig. S3a†). The optical excitation of SPR will lead to the formation of excited electrons on the nanoseed surfaces by continuous 532 nm laser irradiation.[12] The excited electrons can effectively reduce metal ions in solution, providing an additional overgrowth of metal species on irradiated surfaces of the intermediate products. Thanks to the rugged surface structures formed by the enhanced replacement reaction in the early stage, the subsequent overgrowth of Pt and Ag atoms will preferentially occur at protrusion regions, and enable the anisotropic growth process, resulting in the formation of Pt/Ag nanourchins. Compared to Ag^+ ions (originating from the replacement reaction), the reduction of Pt^{2+} ions will dominate the overgrowth process, since some Ag atoms *via* the above reduction process can also be re-oxidized into Ag ions again in the presence of Pt^{2+} ions. This is the main reason for the lower Ag content formed in the final products. The novelty of this synthesis is that the laser-assisted growth process provides enhanced anisotropic chemical reaction on the irradiated surfaces of the nanoseeds. Without any laser beam irradiation in solution, based on a homogeneous replacement reaction between Pt ions and Ag-based nanoseeds as well as the moderate reduction of Pt ions by AA in solution, we found that the products became significantly aggregated/agglomerated and developed into irregular micron-sized materials (Fig. S4†). Moreover, the anisotropic growth is highly related to the laser wavelength and power density. We found that the nanoseeds will develop into quasi-spherical structures instead of urchin-shaped architectures when using 1064 nm laser irradiation in solution (Fig. S3b†). Such incident excitation wavelength in the near-infrared region is not commensurate with SPR (visible region) of the precursors, which inefficiently generates photo-excited electrons. So, the enhanced reduction of metal ions by laser-induced excited electrons also plays an important role in the anisotropic overgrowth process. On the other hand, if a higher power (>500 mW) laser beam was selected in the experiment, aggregated nanomaterials with less obvious nano-protrusions will be formed (Fig. S3c†). The higher laser energy drastically increases the temperature around the nanoseeds, giving rise to an uncontrollable/unpredictable overgrowth process. In summary, the relatively low-power 532 nm laser irradiation of Ag-based nanoseeds would be applicable for the anisotropic growth of Pt/Ag bimetallic nanourchins.

Finally, the fascinating electrocatalytic properties of the as-prepared Pt/Ag bimetallic nanourchins were evaluated (Fig. 6). The typical CVs for different catalysts obtained in 0.5 M H_2SO_4 solution at a sweep rate of 50 mV s^{-1} are shown in Fig. 6a. On the basis of the charge of hydrogen desorption,[24–27] the ECSAs were calculated to reflect the amount of available active sites.[25] As shown in Fig. 6a, there is no hydrogen desorption in the original Ag_2S/Ag nanoparticles (red lines). As for Pt/Ag bimetallic nanourchins and commercial Pt/C (20%), their ECSAs are 13.33 $m^2\ g_{Pt}{}^{-1}$ and 10.71 $m^2\ g_{Pt}{}^{-1}$, respectively. In this way, the Pt/Ag bimetallic nanourchins exhibit excellent ECSA, which is about 1.24 times higher than that of commercial Pt/C (20%) electrocatalyst. More importantly, the novel nanocatalyst also provides pronounced long-term stability during repeated electrochemical tests. As illustrated in Fig. S5a,† the Pt/Ag bimetallic nanourchins show a negligible loss of 0.2% in ECSA after 1500 cycles of the durability tests, which is far better than that of commercial Pt/C catalyst with a significantly loss of about 78.7% after 1000 repeated applications (Fig. S5b†). This pronounced feature is also superior to that of Pd nano-frames reported in recent work.[28] Moreover, the nanoarchitectures were well maintained after 1500 repeated tests, implying the good stability of the obtained Pt/Ag bimetallic nanourchins (Fig. S6†). Then, the MOR was used as a model reaction to elucidate the catalytic performance of catalysts (Fig. 6b). The oxidation peak current for methanol oxidation is observed at ~0.61 V in the presence of catalysts, which is consistent with previous works.[2,7,10] The mass-normalized (mass of Pt) CVs show that the oxidation peak current of methanol on the Pt/Ag bimetallic nanourchins is about 5.2 times higher than that of commercial Pt/C catalyst. In detail, the peak mass current of Pt/Ag bimetallic nanourchins is 302.35 mA $mg_{Pt}{}^{-1}$, while that of commercial Pt/C is 58.17 mA $mg_{Pt}{}^{-1}$. In methanol oxidation, the first anodic peak is usually ascribed to the oxidation of methanol molecules on the electrode surface, while the backward anodic peak is generally attributed to the continuous oxidation of incompletely oxidized carbonaceous intermediates accumulated on the catalyst surface during the forward scan, such as CO, HCOO–, and HCO–.[29] Consequently, the ratio of the forward (I_f) and backward (I_b) peak currents is related to the tolerance of a catalyst to the carbonaceous intermediates

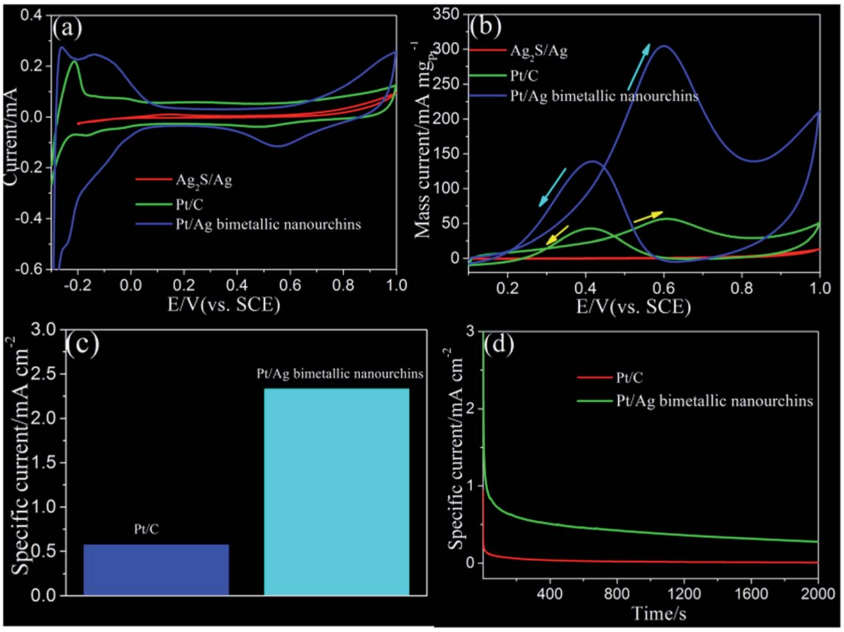

Fig. 6 (a) CVs of Pt/Ag bimetallic nanourchins and commercial Pt/C in 0.5 M H_2SO_4 solution. (b) Pt mass-normalized CV curves for the Pt/Ag bimetallic nanourchins and commercial Pt/C in 0.5 M methanol and 0.5 M H_2SO_4. (c) The specific current of Pt/Ag bimetallic nanourchins and Pt/C in 0.5 M H_2SO_4 and 0.5 M CH_3OH solution. (d) CA curves for the Pt/Ag bimetallic nanourchins and Pt/C in 0.5 M H_2SO_4 and 0.5 M CH_3OH solution. The scan rate for all CVs is 50 mV s^{-1}.

generated during the electro-oxidation of CH_3OH.[30–34] A higher I_f/I_b ratio indicates better decomposition of CH_3OH to CO_2 and H_2O and fewer residual intermediates adsorbed on the surface of the catalyst.[35] In this work, the value of I_f/I_b is about 2.08 for Pt/Ag bimetallic nanourchins, while that of the Pt/C catalyst is 1.32. This observation implies that methanol molecules can be more effectively oxidized on Pt/Ag bimetallic nanourchins during the forward potential scan, generating relatively fewer poisoning species as compared to the commercial Pt/C electrocatalyst. The ECSA-normalized CV curves for Pt/Ag bimetallic nanourchins and commercial Pt/C can be obtained in 0.5 M methanol and 0.5 M H_2SO_4 (Fig. S4c†). Correspondingly, Fig. 6c shows that the specific anodic peak current of the Pt/Ag bimetallic nanourchins is 2.33 mA cm_{Pt}^{-2}, which is much higher than that of commercial Pt/C electrocatalyst of 0.57 mA cm_{Pt}^{-2}. Moreover, the enhanced electrocatalytic activity also exceeds that of some previously reported Pt-based bimetallic nanostructures including Pt–Co nanocrystals (1.07 mA cm_{Pt}^{-2}), Pt–Fe nanocrystals (1.2 mA cm_{Pt}^{-2}), Pt–Cu nanocrystals (1.26 mA cm_{Pt}^{-2}), and Pt–Ni crystals (1.34 mA cm_{Pt}^{-2}).[36] The electrochemical stability of the Pt/Ag bimetallic nanourchins for the MOR was also investigated using CA measurements performed at 0.61 V for 2000 s (Fig. 6d). As shown in Fig. 6d, the CA curves indicate that the current density of the Pt/Ag bimetallic nanourchins is about 0.38 mA cm_{Pt}^{-2}, which is much higher than that of commercial Pt/C electrocatalyst of 0.014 mA cm_{Pt}^{-2} for the entire time course. The obvious comparison further verifies that the Pt/Ag bimetallic nanourchins provide enhanced electrocatalytic performance in MOR application. The fascinating features should be attributed to the unique pronounced intermetallic Pt and Ag synergies including electronic effect, geometric effect, bifunctional mechanism, *etc.*[37–40] Most importantly, without using any polymer stabilizers or soft directing additives, the obtained pure bimetallic Pt/Ag nanourchins with improved electrochemical properties have promising potential as an advanced electrocatalyst for DMFC application.

Conclusion

In conclusion, we have demonstrated the successful synthesis of Pt/Ag (Pt : Ag ∼ 9 : 1) bimetallic nanourchins with mean size of ∼70 nm by laser irradiation of Ag_2S/Ag in K_2PtCl_4 water solution. Based on the laser-induced photothermal effect, the enhanced replacement reaction between Ag species and Pt ions results in the anisotropic deposition of Pt atoms and dissolution of Ag and S ions in solution, giving rise to the formation of intermediate products with rugged surface structures. Then, laser-induced optical excitation of SPR enables excited electrons on the intermediate products to improve the co-reduction of metal ions in solution. The subsequent anisotropic overgrowth of Pt and Ag atoms *via* co-reduction of the two types of metal ions will preferentially occur at protrusion region, resulting in the formation of urchin-shaped structures. The as-prepared Pt/Ag bimetallic nanourchins exhibit pronounced long-term stability in ECSA with a negligible loss of 0.2% even after 1500 repeated tests. This is far better than that of commercial Pt/C electrocatalyst with a loss of 78.7% after 1000 cycles. Interestingly, the obtained novel nanocatalyst provides enhanced electrocatalytic activity and stability for MOR application. The mass-normalized (mass of Pt) CVs show that the peak of mass current is about 302.35 mA mg_{Pt}^{-1}, while that of commercial Pt/C electrocatalyst is 58.17 mA mg_{Pt}^{-1}. As for the electrochemical stability, the CA curves indicate that the current density of the Pt/Ag bimetallic nanourchins is about 0.38 mA cm_{Pt}^{-2}, which is much better than that of commercial Pt/C electrocatalyst of 0.014 mA cm_{Pt}^{-2} for the entire time course (2000 s). It is expected that the pure Pt/Ag bimetallic nanourchins can be used as a promising electrocatalyst for DMFC application.

Conflicts of interest

There are no conflicts to declare.

Acknowledgements

This work was supported by the National Natural Science Foundation of China (No. 11575102, 11105085 and 1175134) and the Fundamental Research Funds of Shandong University (No. 2015JC007).

Notes and references

1 L. Zhang, S. N. Yu and J. J. Gong, *Chem. Sci.*, 2016, **7**, 3500.
2 S. J. Guo, Y. X. Fang, S. J. Dong and E. K. Wang, *J. Phys. Chem. C*, 2007, **111**, 17104.
3 L. T. Sun, H. J. Wang, K. Eid and L. Wang, *Sci. Technol. Adv. Mater.*, 2016, **17**, 58.
4 H. X. Wu, H. J. Li, Y. J. Zhai, X. L. Xu and Y. D. Jin, *Adv. Mater.*, 2012, **24**, 1594.
5 J. T. Zhang, P. P. Liu, H. Y. Ma and Y. Ding, *J. Phys. Chem. C*, 2007, **111**, 10382.
6 L. L. He, P. Song, J. J. Feng, R. Feng, D. X. Yu, J. R. Chen and A. J. Wang, *Electrochim. Acta*, 2016, **200**, 204.
7 L. Wang and Y. Yamauchi, *J. Am. Chem. Soc.*, 2013, **135**, 16762.
8 P. Song, L. Liu, J. J. Feng, J. H. Yuan, A. J. Wang and Q. Q. Xu, *Int. J. Hydrogen Energy*, 2016, **41**, 14058.
9 J. L. Shui, C. Chen and J. C. M. Li, *Adv. Funct. Mater.*, 2011, **21**, 3357.
10 Y. B. He, G. R. Li, Z. L. Wang, Y. N. Ou and Y. X. Tong, *J. Phys. Chem. C*, 2010, **114**, 19175.
11 S. Guo, S. J. Dong and E. Wang, *Chem. Commun.*, 2010, **46**, 1869.
12 D. S. Zhang, B. Gokce and S. Barcikowski, *Chem. Rev.*, 2017, **117**, 3990.
13 M. Grzelczak and L. M. Liz-Marzan, *Chem. Soc. Rev.*, 2014, **43**, 2089.
14 Y. M. Zhai, J. S. DuChene, Y. C. Wang, J. J. Qiu, A. C. Johnston-Peck, B. You, W. X. Guo, B. DiCiaccio, K. Qian, E. W. Zhao, F. Ooi, D. H. Hu, D. Su, E. A. Stach, Z. H. Zhu and W. D. Wei, *Nat. Mater.*, 2016, **15**, 889.
15 X. L. Hu, H. B. Gong, Y. Z. Wang, Q. Chen, J. Zhang, S. H. Zheng, S. K. Yang and B. Q. Cao, *J. Mater. Chem.*, 2012, **22**, 15947.
16 D. L. Liu, C. C. Li, F. Zhou, T. Zhang, H. H. Zhang, X. Y. Li, G. T. Duan, W. P. Cai and Y. Li, *Sci. Rep.*, 2015, **5**, 7686.
17 H. Zhang, M. Chen, D. M. Wang and L. L. Xu, *Opt. Mater. Express*, 2016, **6**, 2573.
18 D. M. Wang, H. Zhang, L. J. Li, M. Chen and X. D. Liu, *Opt. Mater. Express*, 2016, **6**, 1306.
19 S. Li, H. Zhang, L. L. Xu and M. Chen, *Opt. Express*, 2017, **25**, 16204.
20 L. L. Xu, S. Li, H. Zhang, D. M. Wang and M. Chen, *Opt. Express*, 2017, **25**, 7408.
21 S. Pedireddy, H. K. Lee, W. W. Tjiu, I. Y. Phang, H. R. Tan, S. Q. Chua, C. Troadec and X. Y. Ling, *Nat. Commun.*, 2014, **5**, 4947.
22 J. Y. Lee, D. H. Kwak, Y. W. Lee, S. Lee and K. W. Park, *Phys. Chem. Chem. Phys.*, 2015, **17**, 8642.
23 H. Liu, Y. Feng, H. B. Cao and J. Yang, *Nano-Micro Lett.*, 2014, **6**, 252.
24 W. Q. Zhang, J. Z. Yang and X. M. Lu, *ACS Nano*, 2012, **6**, 7397.
25 Y. Q. Cao, Y. Yang, Y. F. Shan, C. L. Fu, N. V. Long, Z. R. Huang, X. X. Guo and M. Nogami, *Nanoscale*, 2015, **7**, 19461.
26 X. W. Liu, W. Y. Wang, H. Li, L. S. Li, G. Zhou, R. Yu, D. S. Wang and Y. D. Li, *Sci. Rep.*, 2013, **3**, 1404.
27 X. W. Du, S. P. Luo, H. Y. Du, M. Tang, X. D. Huang and P. K. Shen, *J. Mater. Chem. A*, 2016, **4**, 1579.
28 Z. N. Wang, H. Wang, Z. R. Zhang, G. Yang, T. N. He, Y. D. Yin and M. S. Jin, *ACS Nano*, 2017, **11**, 163.
29 Y. X. Wang, H. J. Zhou, P. C. Sun and T. H. Chen, *J. Power Sources*, 2014, **245**, 663.
30 Z. L. Liu, X. Y. Ling, X. D. Su and J. Y. Lee, *J. Phys. Chem. B*, 2004, **108**, 8234.
31 Y. Y. Mu, H. P. Liang, J. S. Hu, L. Jiang and L. J. Wan, *J. Phys. Chem. B*, 2005, **109**, 22212.
32 S. J. Guo, Y. X. Fang, S. J. Dong and E. K. Wang, *J. Phys. Chem. C*, 2007, **111**, 17104.
33 Y. Li, W. Gao, L. J. Ci, C. M. Wang and P. M. Ajayan, *Carbon*, 2010, **48**, 1124.
34 P. X. Xi, Y. Cao, F. C. Yang, C. Ma, F. J. Chen, S. Yu, S. Wang, Z. Z. Zeng and X. Zhang, *Nanoscale*, 2013, **5**, 6124.
35 H. S. Fan, M. Cheng, Z. L. Wang and R. M. Wang, *Nano Res.*, 2016, **10**, 187.
36 X. F. Yu, D. S. Wang, Q. Peng and Y. D. Li, *Chem.–Eur. J.*, 2013, **19**, 233–239.
37 D. Zhao, B. Yan and B. Q. Xu, *Electrochem. Commun.*, 2008, **10**, 884.
38 B. M. Concha and M. Chatenet, *Electrochim. Acta*, 2009, **54**, 6130.
39 W. W. He, X. C. Wu, J. B. Liu, K. Zhang, W. G. Chu, L. L. Feng, X. N. Hu, W. Y. Zhou and S. S. Xie, *J. Phys. Chem. C*, 2009, **113**, 10505.
40 K. Kim, K. L. Kim and K. S. Shin, *J. Phys. Chem. C*, 2011, **115**, 23374.